

Mechanism of hypertriglyceridemia in CTP:phosphoethanolamine cytidyltransferase-deficient mice

Ratnesh Kumar Singh,* Morgan D. Fullerton,* Donna Vine,[†] and Marica Bakovic^{1,*}

Department of Human Health & Nutritional Sciences,* University of Guelph, Guelph, Ontario N1G2W1, Canada; Metabolic and Cardiovascular Diseases Laboratory and the Molecular Cell Biology of Lipids Group,[†] University of Alberta, 1-32C Ag/For Centre University of Alberta, Edmonton, Alberta T6G2P5, Canada

Abstract Phosphatidylethanolamine is an important inner-leaflet phospholipid, and CTP:phosphoethanolamine cytidyltransferase-Pcyt2 acts as the main regulator of the de novo phosphatidylethanolamine synthesis from ethanolamine and diacylglycerol. Complete deletion of the mouse *Pcyt2* gene is embryonic lethal, and the single-allele deficiency leads to development of the metabolic syndrome phenotype, including liver steatosis, hypertriglyceridemia, obesity, and insulin resistance. This study aimed to specifically elucidate the mechanisms of hypertriglyceridemia in *Pcyt2* heterozygous mice (*Pcyt2*^{+/-}). Evidence here shows that unlike 8 week-old mice, 32 week- and 42 week-old *Pcyt2*^{+/-} mice experience increased VLDL secretion and liver microsomal triglyceride transfer protein activity. Older *Pcyt2*^{+/-} mice also demonstrate increased levels of postprandial plasma TAGs, increased stimulation of genes responsible for intestinal lipid absorption, transport and chylomicron secretion, and dramatically elevated plasma Angptl4, apoB-100, and apoB-48 content. In addition, plasma HL and LPL activities and TAG clearance following a lipid challenge were significantly reduced in *Pcyt2*^{+/-} mice relative to control littermates. Collectively, these results establish that the hypertriglyceridemia that accompanies *Pcyt2* deficiency is the result of multiple metabolic adaptations, including elevated hepatic and intestinal lipoprotein secretion and stimulated expression and/or activity of genes involved in lipid absorption and transport and lipoprotein assembly, together with reduced plasma TAG clearance and utilization with peripheral tissues.—Singh, R. K., M. D. Fullerton, D. Vine, and M. Bakovic. Mechanism of hypertriglyceridemia in CTP:phosphoethanolamine cytidyltransferase-deficient mice. *J. Lipid Res.* 2012. 53: 1811–1822.

Supplementary key words phospholipid • very low density lipoprotein secretion • chylomicron formation • triglyceride

This work was supported by grants from the Canadian Institutes of Health Research-CIHR (MOP 86448) (M.B.) and NSERC Discovery (D.V.). We declare that CIHR had no involvement in the collection and data analysis, in the interpretation and writing of the manuscript, and in the decision to submit the manuscript for publication.

Manuscript received 25 October 2011 and in revised form 3 July 2012.

Published, JLR Papers in Press, July 4, 2012

DOI 10.1194/jlr.M021881

Copyright © 2012 by the American Society for Biochemistry and Molecular Biology, Inc.

This article is available online at <http://www.jlr.org>

Lipid biosynthesis is essential for the maintenance of cell function and energy homeostasis and defects in lipid metabolism contribute to chronic diseases, including metabolic syndrome, atherosclerosis, and type 2 diabetes. Many studies have also demonstrated that perturbed glucose and FA metabolism are significant risk factors in the development of these pathologies. In contrast, our understanding of how membrane phospholipids contribute in the development of chronic disease is considerably less studied and it is generally poorly understood. There have been select lines of evidence that have highlighted the relationship between phospholipids, mainly phosphatidylcholine (PC) and triglyceride (TAG) metabolism (1–5). FAs released from phospholipid degradation can be utilized for TAG synthesis (2) and changes in membrane PC content are sufficient to cause changes in whole body TAG homeostasis (2, 3). Furthermore, mutations lowering CTP:phosphocholine cytidyltransferase (*Pcyt1*) activity in the PC-Kennedy pathway in Chinese hamster ovary cells result in a redirection of diacylglycerol (DAG) from phospholipids to TAG (3). In *Drosophila*, inhibition of PC synthesis increases TAG content in lipid droplets by altering the size and the morphology of the droplets (1). Evidence from the mouse model with deleted phosphatidylethanolamine (PE) methylation (PEMT) pathway shows that reduced PC synthesis and choline availability could prevent development of high-fat diet-induced obesity (as reviewed in Refs. 4 and 5), and that reduced PC-to-PE membrane ratio contributed to the development of liver steatosis (6, 7) and the endoplasmic reticulum stress in obesity (7).

The specific interaction between PE and TAG metabolism has been largely unexplored. Our laboratory has recently described a mouse model with genetically reduced PE

Abbreviations: AUC, area under the curve; CM, chylomicron; DAG, diacylglycerol; ER, endoplasmic reticulum; FATP, FA transport protein; LSC, liquid scintillation counting; MTP, microsomal triglyceride transfer protein; P407, poloxamer 407; PC phosphatidylcholine; *Pcyt1*, CTP:phosphocholine cytidyltransferase; *Pcyt2*, CTP-phosphoethanolamine cytidyltransferase; PE, phosphatidylethanolamine; PEMT, phosphatidylethanolamine methylation; PS, phosphatidylserine; TAG, triglyceride; TO, triolein;

To whom correspondence should be addressed.
e-mail: mbakovic@uoguelph.ca

de novo synthesis (8) which, similar to the inhibition of PC de novo synthesis in Chinese hamster ovary cells (3), leads to elevated DAG and TAG. Mammalian PE could be synthesized in mitochondria by decarboxylation of phosphatidylserine (PS), but the majority of PE is produced de novo from ethanolamine and DAG through the PE–Kennedy pathway (8–10). In this pathway, ethanolamine is first phosphorylated by ethanolamine kinase to phosphoethanolamine. CTP-phosphoethanolamine cytidylyltransferase (Pcyt2) then catalyzes the formation of CDP-ethanolamine from phosphoethanolamine and CTP, and CDP-ethanolamine and DAG form PE in the final step of the pathway.

Pcyt2 is highly specific and the main regulatory enzyme in the PE–Kennedy pathway (9). Pcyt2 is encoded by a single gene and exists in two catalytically active isoforms, created by alternative splicing (11, 12). Human and murine Pcyt2 are regulated at the transcriptional level by CAAT-box proteins, oxysterols, and LXR, and stimulatory proteins Sp1 and Sp3. Human Pcyt2 is additionally regulated by LXR, EGR1, and NFκB and is downregulated in breast cancer (13–15). Complete deletion of Pcyt2 in mice is embryonic lethal (8), which confirms the essentiality of this gene for animal growth and development. Interestingly, heterozygous mice (*Pcyt2*^{+/-}) mice (16, 17), as well as *Pcyt2* liver-specific knockout mice (18), develop liver steatosis, which establishes a strong physiological connection between PE and TAG syntheses through the common intermediate DAG. To eliminate the excess DAG formed by *Pcyt2* gene deletion, both knockout models synthesize additional FAs from glucose by lipogenesis, and animals inevitably accumulate TAG (16, 18). Further consequences of *Pcyt2* deletion in the systemic heterozygous (*Pcyt2*^{+/-}) mice (16) and the liver-conditional knockout (*Pcyt2*^{l-/-}) mice (18) appear to be deficiencies in PUFAs, typically prevalent in PE, and accumulation of saturated FAs and MUFAs in TAG as a consequence of upregulated lipogenesis. The liver conditional *Pcyt2*^{l-/-} mice also have unmodified plasma lipids (even slightly reduced plasma TAG), suggesting impairments in the liver lipoprotein secretion (18). In the heterozygous *Pcyt2*^{+/-} state, mice have reduced PE synthesis in all tissues, which manifests as a chronic development of metabolic syndrome: the appearance of hepatic steatosis, hypertriglyceridemia, and peripheral insulin resistance at adult stage (16).

The current study was designed to establish the underlying mechanism for the elevated *Pcyt2*^{+/-} plasma TAG (hypertriglyceridemia) that only develops with heterozygous Pcyt2 deficiency. Contrary to expectations, we demonstrate that *Pcyt2*^{+/-} mice have modest (32 week) and highly elevated (42 week) hepatic VLDL secretion, which was previously reported as impaired in the liver-specific *Pcyt2* knockout mice (18). Here, we describe alternative processes that could contribute the *Pcyt2*^{+/-} hypertriglyceridemia, such as liver and intestinal TAG absorption/secretion and postprandial TAG turnover. We demonstrate that *Pcyt2*^{+/-} hypertriglyceridemia is a result of facilitated secretion of both fasting and postabsorptive lipids and an impaired lipolysis and clearance of TAG-rich particles from the circulation. The present investigation contributes

new knowledge as to the importance of proper Pcyt2 function in lipid metabolism and whole-body plasma TAG homeostasis, which may help in the development of new strategies for hypertriglyceridemia.

MATERIALS AND METHODS

Animals

The *Pcyt2*^{+/-} mice of a mixed genetic background (C57Bl/6 × 129/Sv) were generated as described previously (16). Mice were housed under standard conditions with a 12 h light cycle (7.00 AM–7.00 PM), were fed a regular chow diet (Harlan Teklad S-2335), and were given free access to food and water. Experiments were performed on 8, 32, and 42 week-old animals (n = 4–6), after overnight fasting, with food withdrawal at 8.00 PM. The Animal Care Committee of the University of Guelph approved all animal protocols.

Liver VLDL-TAG secretion

Liver TAG secretion was determined in young (8 week) and old (32 week and 42 week) animals. *Pcyt2*^{+/-} and control littermates were injected intravenously with 500 mg/kg of 10% poloxamer 407 (P407) in sterile saline to block plasma LPL activity (19, 20). Blood was sampled via the saphenous vein at baseline, 1, 2, 3, and 4 h, plasma was isolated, and total TAG was determined using standard protocols (Wako Chemicals and Sigma). The rates of hepatic TAG secretion in *Pcyt2*^{+/-} and control littermates were compared by linear regression analysis.

Oral lipid load tolerance test

Pcyt2^{+/-} and wild-type littermates were fasted overnight and were given an intragastric load of 200 μl of olive oil. The mice were anesthetized with isoflurane, and blood was collected at different time points via the retro-orbital plexus immediately after the lipid load and 1–6 h after the load. Plasma TAG content was determined using a standard kit from Sigma. Differences in TAG turnover between two genotypes were determined by integration of TAG content during the entire postload period, after which the differences in the area under the curve (AUC) were compared between the genotypes.

Intestinal chylomicron-TAG secretion

Pcyt2^{+/-} and wild-type littermates were injected intravenously with 500 mg/kg of 10% P407. Subsequently, mice were given an intragastric load of 10 μCi of [³H] triolein (TO) in 200 μl of olive oil. Blood samples were collected via the retro-orbital plexus immediately after the lipid load (15 min) and 1, 2, and 3 h after the load. Lipids were extracted from plasma according to the method of Bligh and Dyer (21). [³H]TAG lipids were separated from other components by TLC using a solvent system of heptane-diethyl ether-acetic acid (60:40:3), and the [³H] radioactivity in the TAG fractions was determined by liquid scintillation counting (LSC) as previously described (16).

Analysis of intestinally secreted lipids

Pcyt2^{+/-} and wild-type littermates were injected with 500 mg/kg of 10% P407 and were given an intragastric [³H]TO fat load as above. Lipids were extracted from the small intestinal mucus at 30 min and 3 h, and from 1 h plasma, according to the method of Bligh and Dyer (21). [³H] radiolabeled TAG, DAG, FFAs, total cholesterol, and total phospholipids were separated and characterized by LSC as we have previously described (16, 17).

Analysis of intestinal lipids

TAG and DAG content of *Pcyt2*^{+/-} and wild-type intestinal mucosa was determined after isolation and separation on Silica gel-60 TLC plates using hexane-diethyl ether-acetic acid (60:40:3 v/v)

and visualization with iodine vapor. TAG and DAG content in *Pcyt2*-deficient mice relative to wild-type mice were determined by densitometry (16). Total intestinal TAG content (nmol/mg) was determined by the TAG fluorometric assay kit from Abcam.

Plasma clearance of TAG-rich particles

Radiolabeled TAG-rich particles were prepared by sonication of 75 μCi of [^3H]TO in 100 mg of a lipid emulsion containing 23:70:2:3:2 v/v ratio of PC, “cold” triolein, lyso-PC, cholesteryl oleate, and cholesterol (22, 23). The sonicated lipid particles were stored at 4°C and used within 7 days after preparation. Degradation of the radiolabeled TAG-rich particles was followed in *Pcyt2*^{-/-} and wild-type littermates after an intravenous injection of 100 μg of the radiolabeled emulsion. The blood (50 μl) was collected at 2, 5, 10, 15, and 30 min after injection. Total plasma [^3H] radioactivity was determined as described above and expressed as a fraction of the injected dose of the [^3H]TO-labeled particles (100%) (22, 23).

Tissue uptake of TAG-rich particles

Lipid distribution into various tissues was determined at the end of the plasma clearance assay, 30 min after the [^3H]TO injection described above. Various tissues (liver, heart, muscle, adipose, kidney, spleen) from *Pcyt2*^{-/-} mice and wild-type littermates were collected, weighed and dissolved in Soluene (PerkinElmer) by an overnight incubation at 70°C (23). The [^3H] radioactivity was determined in identical amounts of homogenized tissues. The incorporated [^3H] activity was expressed as a % of the injected dose/g weight and compared between the genotypes as described (23).

Plasma LPL and HL activity assays

Fasted *Pcyt2*^{-/-} mice and wild-type littermates were injected via the retro-orbital plexus with 0.1 U/g of heparin, and the postheparin plasma was collected after 30 min. HL and LPL activities were determined as described (22, 23). The radiolabeled substrate was prepared by sonication of 2.5 $\mu\text{Ci/ml}$ [^3H]TO with “cold” TO (4.6 mg/ml), FA-free BSA (20 mg/ml), Triton X-100 (0.1%), and heat-inactivated human serum in 0.1 M Tris-HCl buffer (pH 8.6). Ten microliters of the mouse plasma was incubated with 0.2 ml of the sonicated substrate for 30 min at 37°C in the presence (HL activity) and in the absence (total lipase activity) of 1 M NaCl. NaCl inhibits LPL activity and has only a minor effect on HL activity. The reaction was stopped by 3 ml of heptane-methanol-chloroform (1:1.3:1.4) and diluted with 1 ml of 0.1 M K₂CO₃/saturated boric acid buffer (pH 10.5). The water phase, which contained the released product [^3H]oleate, was separated by centrifugation (5 min at 3,000 rpm), and 0.5 ml of the water fraction was counted. The HL activity was calculated as part of total activity that was not inhibited by NaCl, whereas the LPL activity represented the remaining activity. Both activities were expressed as [oleate] nmol/h/ml.

Expression analysis of LPL and angiopoietin-like protein 4

Total mRNA was isolated from 50 mg of homogenized tissues (liver, muscle, heart, intestine, and adipose) using Trizol reagent (Invitrogen). First-strand cDNA was generated from 2 μg of total RNA, and PCR was performed using the LPL-specific primers 5'-GCTCG-CACGAGCGCTCCATT-3' (forward) and 5'-CCTCGGGCAGGGTG-AAGGGAA-3' (reverse). A G3PDH PCR product was used as internal control. Angiopoietin-like protein 4 (*Angptl4*) was determined in 10 μg of total plasma by Western blotting using an *Angptl4*-specific antibody (#40-9800) from Invitrogen. The band intensities of the LPL PCR product and *Angptl4* protein were analyzed by the ImageJ software.

Determination of plasma apoB-48 content

Pcyt2^{-/-} and wild-type littermates were fasted overnight. Subsequently, mice were given an intragastric load of 200 μl of olive oil,

and blood samples were drawn 3 h after gavage via the retro-orbital plexus. The plasma was snap-frozen and stored at -80°C until analysis. Plasma apoB-48 concentration was quantified using an adapted Western immune blot method, as previously described (24). Briefly, total plasma was separated by SDS-PAGE on a 3–8% tris-acetate polyacrylamide NuPage® gel (Invitrogen). Separated proteins were transferred to a polyvinylidene fluoride membrane (0.45 μM ; ImmobilonP™, Millipore). Membranes were incubated with a goat polyclonal antibody to apo-B (1:100; Santa Cruz Biotech). Detection was achieved using an anti-goat secondary antibody and chemiluminescence (ECL Advance; Amersham Biosciences, UK); intensity was quantified using linear densitometric comparison with a known mass of purified rodent apoB-48 protein.

MTP activity assay

Liver and small intestine from *Pcyt2*^{-/-} mice and control littermates were homogenized in 10 mM Tris-HCl (pH 7.4), 150 mM NaCl, 1 mM EDTA, and 2% protease inhibitor cocktail (Sigma-Aldrich) (25). The microsomal triglyceride transfer protein (MTP) activity was measured using a fluorometric activity assay from Roar Biomedical.

Intestinal gene expression

The small intestine from *Pcyt2*^{-/-} mice and control littermates was excised and washed with cold isotonic saline solution to remove excess blood. The intestinal lumen was flushed with saline to remove digested food particles, the wall was scraped out with a glass slide, and mucosal tissue was collected in liquid nitrogen. Total RNA isolation and cDNA synthesis was performed as above. Specific primers to measure the expression of intestinal genes MTP, CD46, FATP4, FAS, DGAT1/2, MGAT2, and SREBP1 were used. The PCR conditions and the gene-specific primers used in this analysis can be obtained upon request.

Preparation of radiolabeled enterocytes

Pcyt2^{-/-} mice and wild-type littermates were fasted overnight and given an intragastric load of 10 μCi of [^3H]TO in 200 μl of olive oil. The enterocytes were isolated from the intestinal lumen 15 min after the lipid load, as previously described (26–28). The intestinal lumen was first washed with Solution-I (115 mM NaCl, 5 mM KCl, 0.96 mM NaH₂PO₄, 26 mM NaHCO₃, and 5.5 mM glucose, pH 7.4) and gassed with 95% O₂ for 20 min. The small intestine was then filled up with Solution-II (67.5 mM NaCl, 1.5 mM KCl, 0.96 mM NaH₂PO₄, 26.19 mM NaHCO₃, 27 mM sodium citrate, and 5.5 mM glucose, pH 7.4) and incubated at 37°C in oxygenated 0.9% saline, with constant shaking. The luminal solution was discarded after 15 min of incubation, and the small intestine was filled up with Solution III (115 mM NaCl, 5 mM KCl, 0.96 mM NaH₂PO₄, 26 mM NaHCO₃, 1.5 mM EDTA, 5.5 mM glucose, 0.5 mM dithiothreitol, pH 7.4), and again incubated for 15 min in aerated 0.9% saline. The luminal content was then collected and centrifuged (5 min; 1,500 rpm; room temperature), and the isolated enterocyte pellet was resuspended in the aerated DMEM. To collect secreted lipoproteins, enterocytes were incubated in the fresh DMEM for 3 h. The lipoprotein particles secreted from enterocytes were collected from the media by sequential density gradient ultracentrifugation, and the radiolabeled lipids in each lipoprotein fraction were determined by LSC.

Density centrifugation of in vitro-secreted intestinal lipoproteins

Sequential density gradient centrifugation was performed on the lipoproteins isolated from enterocytes 15 min after the fat load, and the lipoproteins were secreted from the isolated enterocytes after 3 h incubation. Separation of the large chylomicrons

(CM_L), small chylomicrons (CM_{SM}), and the VLDL-like chylomicron particles (CM_{VLDL}) was performed as previously described (28–30). Media or enterocyte protein homogenates were mixed with 2 ml of 1.006 g/ml-density solution containing 0.57 g/ml KBr, to obtain a final density of 1.10 g/ml. The mixture was overlaid with 3 ml each of 1.063 g/ml- and 1.019 g/ml-density solution and 2 ml of 1.006 g/ml-density solution and subjected to sequential centrifugation. Large chylomicrons (CM_L) were obtained from the top 1 ml layer after the first centrifugation (33 min, 40,000 rpm, at 15°C using the SW41 rotor). The remaining solution was overlaid with 1 ml of fresh 1.006 g/ml solution and subjected to the second ultracentrifugation (3.5 h, 40,000 rpm, 15°C). The second top 1 ml layer contained the small chylomicron (CM_{SM}) particles. After adding a new 1 ml of 1.006 g/ml solution, the samples were subjected to the third ultracentrifugation (17.5 h, 40,000 rpm, 15°C), of which the 1 ml top fraction represented the CM_{VLDL} ($d < 1.006$ g/ml) particles. The rest of the gradient was fractionated into 1.5 ml portions. CM fractions 1–3 represented the range similar to the LDL size (CM_{LDL} ; $d = 1.02$ – 1.063 g/ml), and fractions 4–6 represented the range of the HDL (1.063–1.1 g/ml). Total [3H] lipids in all fractions was determined by LSC and the lipoprotein profiles compared between $Pcyt2^{+/-}$ and wild-type littermates.

Density centrifugation of in vivo-secreted intestinal lipoproteins

Plasma from $Pcyt2^{+/-}$ and wild-type littermates was collected 1 h after the [3H]TO lipid load, and 100 μ l was subjected to density gradient centrifugation as described above for the in vitro experiments. Total [3H] radioactivity in various lipoprotein fractions was determined by LSC and the distribution profiles compared between $Pcyt2^{+/-}$ and wild-type littermates as described above.

Statistical analysis

Results were expressed as mean \pm SD. Statistical analysis was done using the Student paired *t*-test, the exponential curve fit, and the linear regression analysis using Graph Pad Prism software. Values of $P < 0.05$ were considered statistically significant.

RESULTS

Liver TAG secretion was elevated in older $Pcyt2^{+/-}$ mice

We demonstrated previously that $Pcyt2^{+/-}$ mice develop insulin resistance, elevated plasma VLDL particles, and hypertriglyceridemia at 32–36 weeks of age (16). Young $Pcyt2^{+/-}$ mice (8 week-old) had normal plasma glucose, insulin, and lipoprotein content (16). Therefore, we first investigated whether the VLDL secretion was a contributing factor to the increased plasma TAG observed in older $Pcyt2^{+/-}$ mice. Plasma TAG content (Fig. 1A) and liver MTP activity and expression (Fig. 1B, C) were determined in 8, 32, and 42 week-old $Pcyt2^{+/-}$ mice. VLDL secretion was not significantly different between the 8 week-old $Pcyt2^{+/-}$ mice and wild-type littermates. At 32 weeks of age, however, $Pcyt2^{+/-}$ mice showed an increased TAG secretion, which was further elevated at 42 weeks of age (Fig. 1A). Liver MTP activity and expression correspondingly increased 1.8–2-fold in 32 and 42 week-old $Pcyt2^{+/-}$ mice while remaining normal in 8 week-old $Pcyt2^{+/-}$ mice (Fig. 1B, C). These results collectively established that $Pcyt2$ deficiency produced an age-dependent upregulation of VLDL secretion that contributed to the elevated plasma VLDL and hypertriglyceridemia in older $Pcyt2^{+/-}$ mice

(16). All additional experiments were performed with the hypertriglyceridemic 42 week-old $Pcyt2^{+/-}$ mice.

Postprandial TAG turnover is reduced in $Pcyt2^{+/-}$ mice

We next determined whether the $Pcyt2^{+/-}$ mice had any defects in the absorption and processing of postprandial lipids. TAG content in the plasma was followed after animals were given an intragastric bolus of olive oil, as shown in Fig. 2A, B. $Pcyt2$ -deficient mice exhibited a faster appearance of TAG in the plasma, and this was maintained at levels higher and longer than in control littermates. Based on the AUC, the quantitative difference in the postprandial TAG responses between deficient and control animals was 40% (Fig. 2B), showing that the $Pcyt2^{+/-}$ mice had both an increased intestinal secretion and a delayed TAG clearance from the plasma, and those two aspects of $Pcyt2^{+/-}$ hypertriglyceridemia were separately examined using a radiolabeled TAG substrate ([3H]TO) as described below.

Intestinal TAG secretion is elevated in $Pcyt2^{+/-}$ mice

To investigate the extent to which intestinal secretion may contribute to $Pcyt2^{+/-}$ hypertriglyceridemia, the animals were intravenously injected with the lipase inhibitor P407 as above and then given an intragastric load of labeled olive oil. The secretion of intestinal lipids was monitored by the appearance of 3H -related activity in the plasma TAG at various times after the lipid load. As shown in Fig. 2C, both groups of animals displayed a continuous appearance of the radiolabeled TAG in the plasma when measurements were performed for 3 h after lipid load; however, more [3H] activity appeared in the plasma of $Pcyt2^{+/-}$ animals compared with control littermates. This was a strong indication that $Pcyt2$ -deficient intestinal epithelia had acquired an accelerated secretion of the postprandial lipids.

Postprandial lipids in intestinal mucosa and plasma were investigated in the presence of the lipase inhibitor to prevent plasma degradation, as described above. As expected, most radiolabeled lipids were in the form of [3H] TAG in both types of animals (Fig. 3A–C). After 1 h of lipid load, $Pcyt2^{+/-}$ intestinal mucosa had elevated (40%) radioactivity in TAG, DAG, and FFA fractions and 20–30% increase in other lipids (Fig. 3B). In 3 h plasma, the [3H] TAG activity was similar to the activities in the intestinal mucosa, containing \sim 40% more label in $Pcyt2^{+/-}$ plasma than in the wild-type plasma. Postprandial [3H]DAG and [3H]FFAs were 2-fold higher in the $Pcyt2^{+/-}$ plasma compared with wild-type (Fig. 3C). A 2–3-fold ratio between [3H] TAG and [3H]DAG was associated with all measurements shown in Fig. 3A–C. We showed previously that the major underlying mechanism of disease progression in $Pcyt2^{+/-}$ mice was a shift in lipid and energy metabolism to remove excess DAG and TAG unused in the PE–Kennedy pathway. This results in elevated lipogenesis and TAG synthesis even early in development and causes age-related accumulation of lipids in adipocytes, liver, muscle, and perhaps other organs (8, 16, 17). The actual TAG content (Fig. 3D) and the relative change in TAG and DAG (Fig. 3E) were 1.8–2.3-fold higher in the intestinal mucosa of $Pcyt2^{+/-}$ mice compared with littermate controls, demonstrating that in addition to

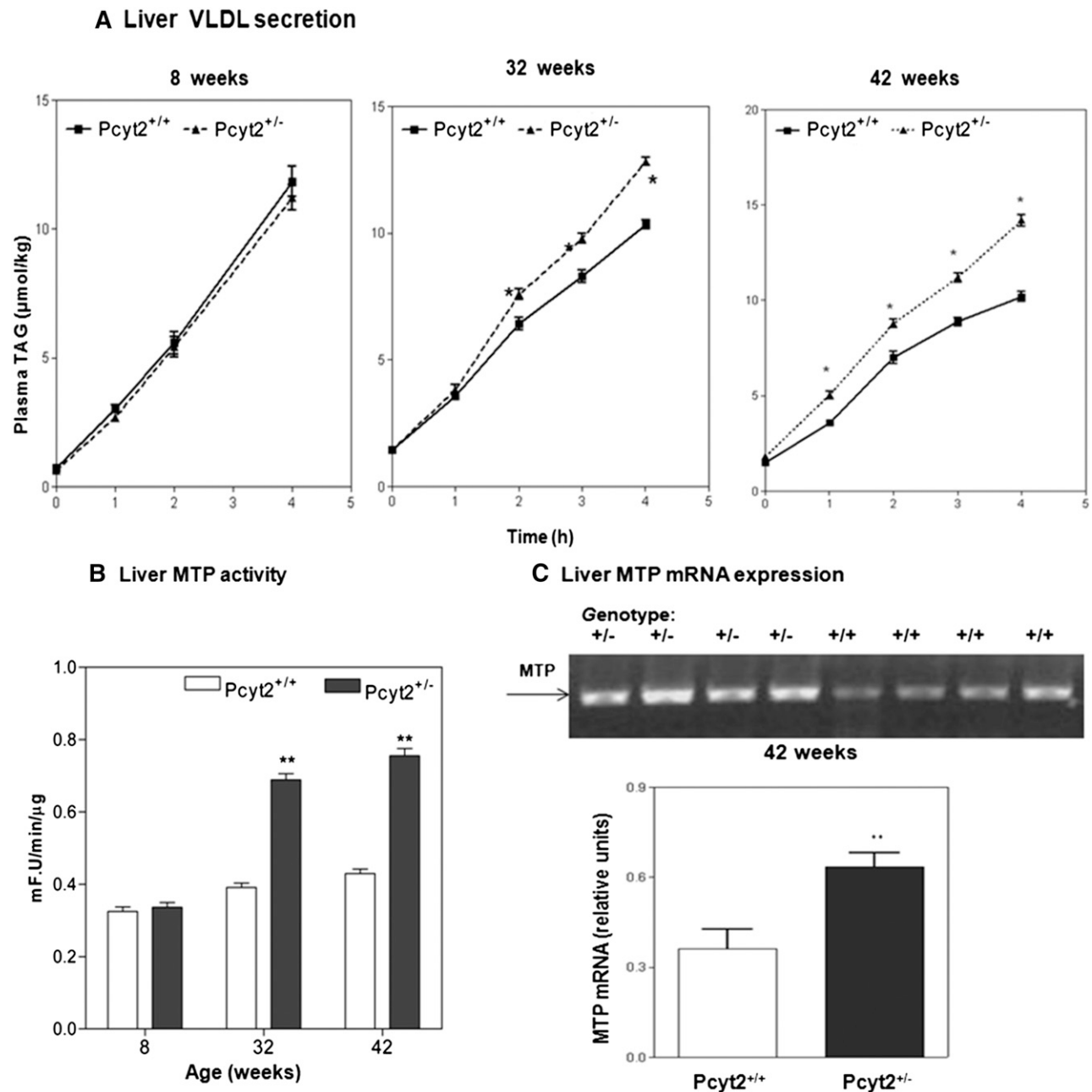


Fig. 1. Age-dependent stimulation of VLDL secretion and liver MTP activity in *Pcyt2*^{+/-} mice. A: Fasting plasma TAG was measured in 8, 32, and 42 week-old *Pcyt2*^{+/-} mice and littermate controls. Plasma LPL was inhibited with P407 injection, and VLDL-TAG was determined in 0–4 h intervals. At 8 weeks of age, VLDL-TAG secretion was similar in *Pcyt2*^{+/-} mice and control littermates. A modest but significant increase in VLDL secretion was present in 32-week-old *Pcyt2*^{+/-} mice; and 42-week-old *Pcyt2*^{+/-} mice showed significantly elevated VLDL secretion compared to littermates. The level of activity (B) and expression (C) of the liver MTP in 8, 32, and 42 week-old mice. MTP activity was expressed as fluorescence (F) U.min⁻¹.µg of protein⁻¹ for n = 5 mice in each group. Statistical significance (* and **) at each point was determined by Student's t-test at *P* < 0.05.

accumulation and increased secretion of hepatic lipids in postabsorptive states, *Pcyt2*^{+/-} mice also have increased intestinal lipids and secretion in postprandial states.

Plasma clearance of TAG-rich particles is impaired in *Pcyt2*^{+/-} mice

To establish whether impaired degradation of plasma TAG also contributed to the *Pcyt2*^{+/-} hypertriglyceridemia, animals were injected with labeled TAG-rich lipid particles, and the particle disappearance from circulation was monitored. As

evinced from the relative radioactivity remaining in the plasma, shown in Fig. 4A, the rate of disappearance of the [³H]TO-labeled lipids was markedly slower in the *Pcyt2*^{+/-} mice (the half-life, *t*_{1/2} = 43.30 min⁻¹) than in the littermate controls (the half-life, *t*_{1/2} = 5.17 min⁻¹), indicating inefficient hydrolysis of both VLDL and CM in the heterozygous mice.

Total lipid uptake in various tissues was examined 30 min after the [³H]TAG particle injection (Fig. 4B). The associated tissue radioactivity was 50–60% lower in *Pcyt2*^{+/-} liver, total adipose tissue, and kidney and significantly

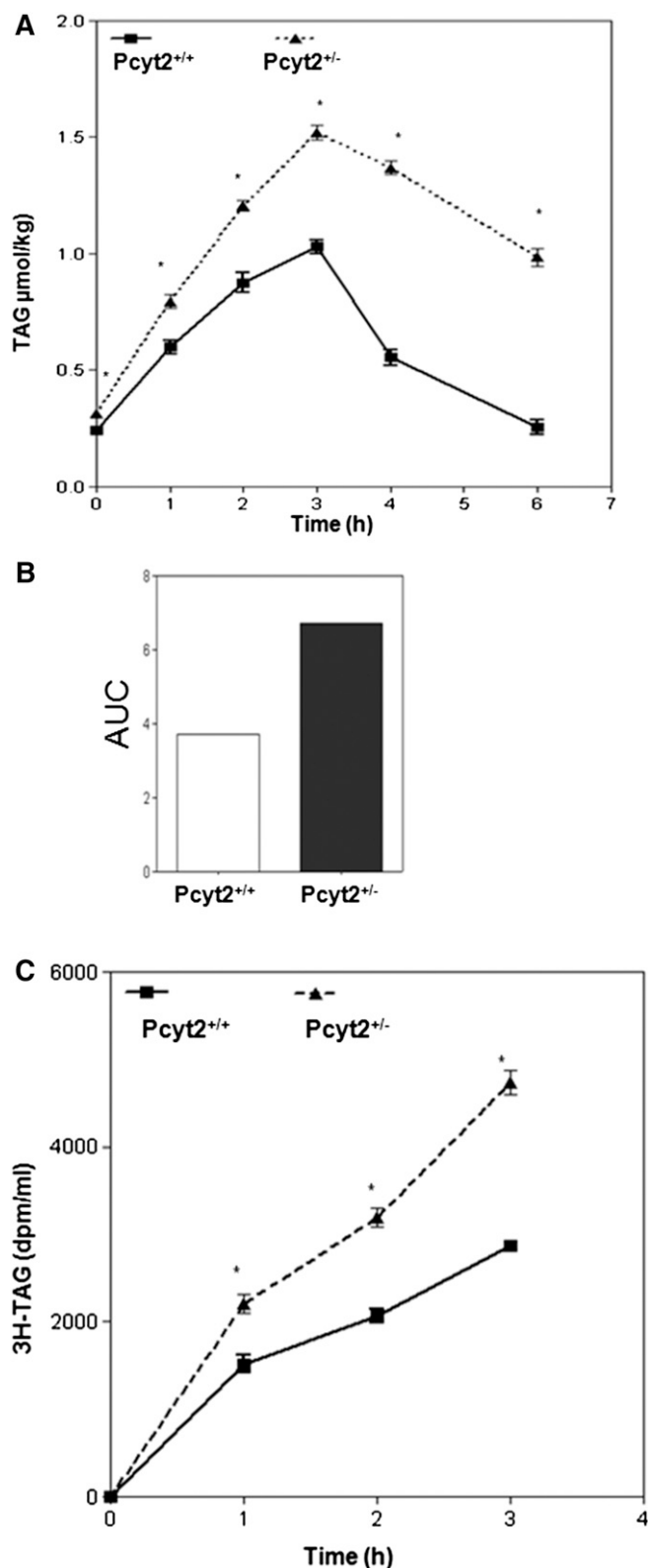


Fig. 2. *Pcyt2* deficiency modifies postprandial lipid response. Plasma TAG turnover is reduced (A). *Pcyt2*^{+/-} and littermate (*Pcyt2*^{+/+}) control mice were given an intragastric bolus of 200 μ l of olive oil, and a blood sample was drawn at 0, 1, 2, 3, 4, and 6 h after the lipid load. Total plasma lipid content was expressed as TAG (μ mol/kg) \pm SD for four mice per group. Shown in B is the integrated AUC of data in A for both wild-type and knockout animals. C: Intestinal TAG secretion is increased. *Pcyt2*^{+/-} and littermate

reduced in total skeletal muscle and heart relative to control tissue homogenates. Taken together, these data indicate that *Pcyt2*^{+/-} mice acquire an impaired clearance of TAG-rich particles from the plasma; therefore, we next investigated lipase activity in *Pcyt2*-deficient tissues.

Plasma LPL and HL activities are reduced in *Pcyt2*^{+/-} mice

Reduced postprandial TAG turnover (Fig. 2A, B) and delayed TAG particle clearance (Fig. 4A) from *Pcyt2*^{+/-} circulation were both consistent with decreased plasma lipolysis, mainly controlled by the plasma LPL and HL activities. To investigate this, lipase activities were measured in the postheparin plasma of both genotypes. As shown in Fig. 4C, the total plasma lipase (33%) and individual LPL (44%) and HL (27%) activities were significantly reduced in the *Pcyt2*^{+/-} plasma compared with control plasma.

Altered expression of LPL and angiopoietin-like protein 4

We next investigated whether decreased tissue LPL availability may contribute to the reduced activity in *Pcyt2*^{+/-} mice. LPL is mainly expressed in adipose tissue and to some extent in skeletal muscle and heart. LPL mRNA was completely absent from intestine and unchanged in the total skeletal muscle and liver of *Pcyt2*^{+/-} mice. On the other hand, *Pcyt2*^{+/-} adipose tissue and heart homogenates had 1.7- and 1.5-fold less LPL mRNA (Fig. 5A, B). Angptl4 is a very potent inhibitor of LPL activity and a stimulator of adipose tissue lipolysis (31), and, as shown in Fig. 5C, D, there is a marked 1.97-fold increase in the expression of serum Angptl4 in *Pcyt2*^{+/-} mice relative to control littermates. Therefore, both reduced LPL tissue expression and increased LPL inhibition contributed to the reduced LPL activity in the *Pcyt2*^{+/-} plasma.

Plasma apoB and intestinal MTP activity are elevated in *Pcyt2*^{+/-} mice

The lipid tolerance test (Fig. 2A) established a significant postprandial contribution to plasma *Pcyt2*^{+/-} TAG, therefore the postprandial apoB lipoprotein content was also determined. As shown in Fig. 6A–C, apoB-100 and apoB-48 content was dramatically increased, with apoB-48 levels 5-fold and apoB-100 levels 1.8-fold higher than in the control plasma. The elevation in plasma apoB proteins is consistent with the increased VLDL secretion (Fig. 1A) and with the previously established accumulation of the VLDL particles in *Pcyt2*^{+/-} plasma (16). To confirm that intestinal lipoprotein production was elevated in *Pcyt2* deficiency, we also measured the intestinal MTP activity in 42 week-old mice. As shown in Fig. 6D, the MTP activity was elevated 3-fold, demonstrating that *Pcyt2*^{+/-} mice also produced more lipoprotein (chylomicron) particles in the small intestine.

controls were injected intravenously with 500 mg/kg of 10% P407 LPL inhibitor and were immediately given an intragastric load of [³H]TO in 200 μ l of olive oil as in A. Blood samples were drawn at 0, 1, 2, and 3 h, and total lipids were extracted from plasma. Shown is the [³H] radioactivity in TAG fraction for four mice in each group. Statistical significance (*) at each point was determined by Student's *t*-test at *P* < 0.05.

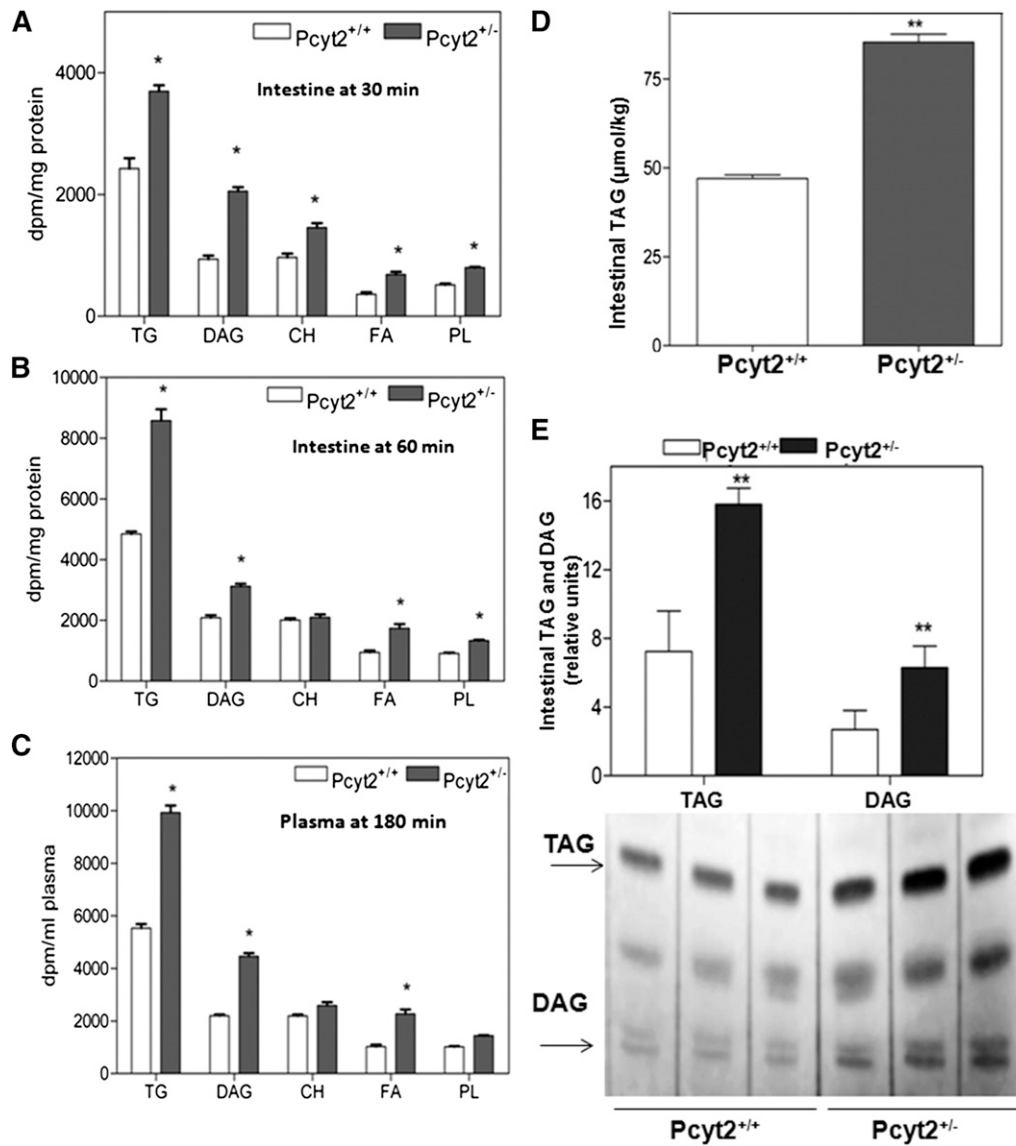


Fig. 3. Differences in intestinal lipids and secretion. A: Intestinal profiles of TAG, DAG, FFAs (FA), total cholesterol (CH), and total phospholipids (PL) 30 min and (B) 60 min after the [³H]TO-containing fat load. C: Plasma lipid profiles 180 min after the [³H]TO lipid load. *Pcyt2*^{+/-} and *Pcyt2*^{+/+} (n = 5). The values shown in A and B are dpm/mg of protein for intestinal mucosa and in C are dpm/ml for mouse plasma at *P* < 0.05. D: Intestinal mucosa TAG (μmol/kg) is elevated 1.8-fold in *Pcyt2*^{+/-} mice relative to the wild-type mice (40 wk-old; n = 4 and *P* < 0.0001). E: Iodine-stained silica gel showing relative increases in DAG and TAG levels (2.3-fold and 1.9-fold, respectively) in the samples as in D.

Chylomicron production and secretion are upregulated in *Pcyt2*^{+/-} mice

To gain further insight into the mechanism of elevated postprandial TAG and apoB containing lipoproteins in *Pcyt2*^{+/-} plasma, we next examined the postprandial profiles of lipoproteins secreted *in vitro* from isolated enterocytes and *in vivo* from intestine (Fig. 7). We conducted a density lipoprotein centrifugation to separate various lipoproteins and to correlate the extent of lipidation within different fractions from the primary enterocytes (Fig. 7A), those secreted into the media (Fig. 7B), and those secreted *in vivo* (Fig. 7C). For both genotypes, the absorbed lipids were associated with similar lipoprotein fractions and were in a descending order from CM_L=CM_LLDL>CM_S=HDL>CM_{VLDL}.

However, the enterocytes isolated from *Pcyt2*^{+/-} intestine contained proportionally 30–50% more lipids compared with control cells in all lipoprotein fractions (Fig. 7A). This directly demonstrates that the intestinal absorption was significantly increased in the *Pcyt2*^{+/-} mice. To investigate the secretion phase, the isolated enterocytes were incubated for 3 h, and the lipoproteins secreted into media were examined. The type and the order of the secreted lipoproteins was similar in both genotypes, and it was dominated by large and small CM fractions, CM_L>CM_S>CM_{LDL}>HDL = CM_{VLDL}. The most-abundant fractions, CM_L and CM_S, had >2-fold more lipids in the *Pcyt2*^{+/-} enterocyte media than the CM_L and CM_S fractions isolated from the control media (Fig. 7B). Finally, the

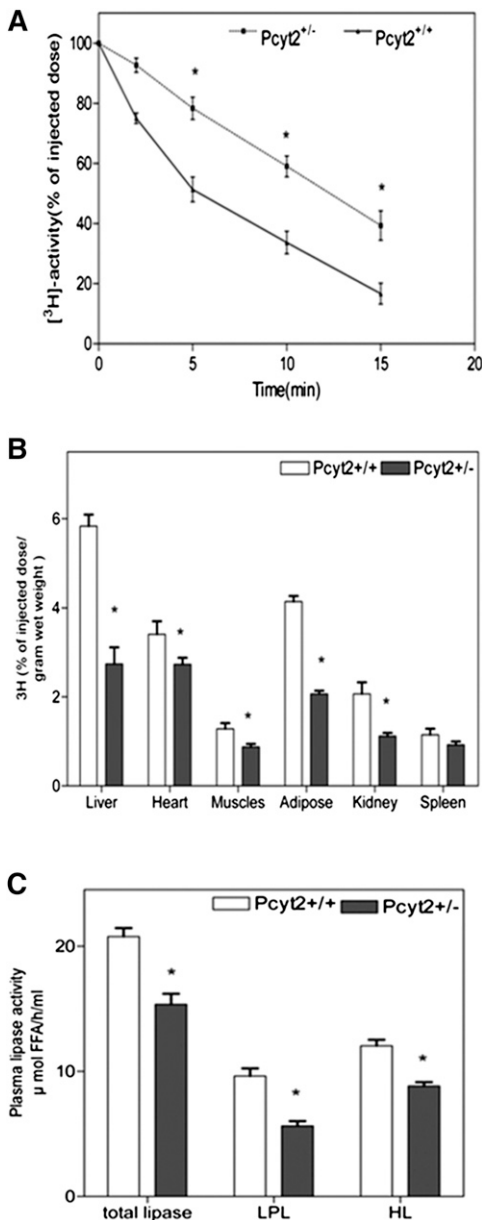


Fig. 4. Pcyt2 deficiency inhibits plasma lipid clearance. **A:** Clearance of TAG-rich lipid particles is reduced in Pcyt2^{+/-} plasma. [³H] TO (100 µg of total TAG) was injected in Pcyt2^{+/-} and littermate controls via the inferior vena cava, and blood samples were taken at various times (2.5–15 min) postinjection. Plasma radioactivity (dpm) was determined and expressed as a percent of the injected dose vs. time (min); n = 4 in each group. **B:** Delivery of TAG-rich lipid particles is reduced in multiple Pcyt2^{+/-} tissues. [³H]TO particles (100 µg of TAG) were injected as in A, and radioactivity (dpm) was determined at 30 min in homogenized tissues (liver, heart, muscle, adipose, kidney, and spleen). Data are shown as a percent of the injected dose/g weight for four animals; *P < 0.05. **C:** Pcyt2^{+/-} mice have impaired plasma HL and LPL activities. Fasted Pcyt2^{+/-} and wild-type mice were injected via retro-orbital plexus with heparin (0.1 U/g), and blood was collected 20 min after injection. Plasma was incubated for 30 min at 37°C with a [³H] TO in the absence or presence of 1 M NaCl to establish both the LPL and HL activity. Generated [³H] oleate was extracted, and activity was determined as [oleate] µmol/h/g tissue ± SD (n = 4) at *P < 0.05.

plasma lipoproteins secreted in vivo were fractionated (Fig. 7C). The extent of lipidation of CM fractions was similar to those observed for enterocyte media, and Pcyt2^{+/-} plasma CM_L and CM_S fractions again contained >2-fold more lipids than the CM_L and CM_S from the control plasma. Not surprisingly, plasma CM_{LDL} and HDL fractions were more abundant than those obtained in the enterocyte media, but the lipid content was similar in vitro and in vivo, and it was higher in the CM_{LDL} and HDL-like fractions isolated from the Pcyt2^{+/-} than in the wild-type plasma.

Pcyt2^{+/-} intestinal genes for FA absorption and chylomicron formation are upregulated

To further determine the mechanism for the elevated Pcyt2^{+/-} intestinal lipid absorption and chylomicron secretion, the genes associated with FA transport, TAG synthesis, and chylomicron assembly were examined in both genotypes, as shown in Fig. 8. We found that postprandial mRNA expression of FA transport protein 4 (FATP4), the only FATP in the intestine, was 3-fold higher and that the main enterocyte FA transporter, CD36, was 2-fold higher in Pcyt2^{+/-} small intestine than in control littermates. The expression of MTP, which has a critical role in chylomicron assembly, was also 2-fold higher in Pcyt2^{+/-} intestine. Interestingly, the genes involved in intracellular TAG formation, DGAT1, and DGAT2 did not change significantly, and they probably are more regulated by post-translational mechanisms such as phosphorylation (32). FA synthesis normally is not a major event in this tissue, but could potentially be modified in insulin resistance and diabetes (32, 33). The postprandial expression of the main lipogenic genes SREBP1 and FAS were dramatically reduced (3-fold and 2.8-fold, respectively) showing that enterocyte de novo synthesis of FA was reduced in Pcyt2^{+/-} mice. Therefore, the FA pool available for the increased TAG formation and chylomicron assembly in Pcyt2^{+/-} intestine was produced by increased uptake and intracellular transport of dietary FAs (33).

DISCUSSION

Pcyt2 regulates de novo PE phospholipid synthesis, an anabolic pathway that utilizes ATP and DAG. The attenuation of this pathway in Pcyt2^{+/-} mice creates a surplus of those metabolites and reduces demands for energy production by mitochondrial FA oxidation. Indeed, young Pcyt2^{+/-} mice experience reduced weight loss after prolonged fasting and have upregulated liver lipogenesis prior to development of obesity, insulin resistance, and hyperlipidemia (16). Therefore, the redistribution of DAG/FAs from membrane PE toward TAG creates a state of positive energy balance in Pcyt2 deficiency. These inherent changes, in combination with the age-related decline in metabolic efficiency (34, 35) and changes in energy and nutrient signaling networks (36, 37) are probably most responsible for the disease progression in this model.

In the present study, we focused on Pcyt2^{+/-} hyperlipidemia that developed in older animals. We established that Pcyt2^{+/-} hyperlipidemia was a net result of increased secretion of TAG-rich lipoproteins and reduced capacity for lipid clearance from the plasma. Furthermore, there

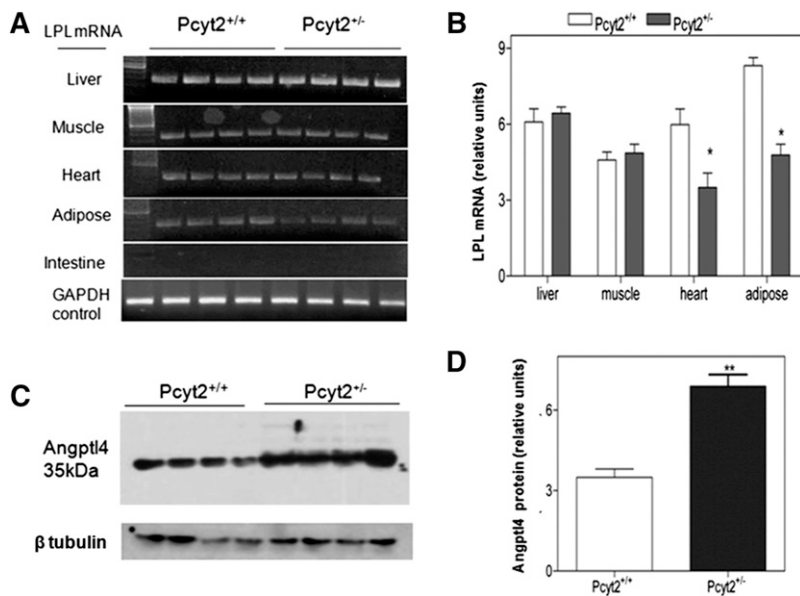


Fig. 5. *Pcyt2*^{-/-} mice have reduced tissue LPL and increased plasma Angptl4. A: PCR results for LPL mRNA expression in various tissues of *Pcyt2*^{-/-} and littermate control mice (n = 4). B: LPL mRNA levels relative to control G3PDH showing significantly reduced LPL expression in homogenates of *Pcyt2*^{-/-} heart (1.5-fold, *P* < 0.002) and adipose (1.74-fold, *P* < 0.0006) and no change in skeletal muscle and liver total homogenates. Immunoblots (C) and densitometric analysis (D) showing increased amounts of Angptl4 protein in *Pcyt2*^{-/-} plasma relative to control plasma (1.97-fold, *P* < 0.0007, n = 4).

was a strong relationship between *Pcyt2* deficiency and the activity and expression of genes involved in plasma lipolysis and intestinal lipid absorption and secretion, uncovering for the first time that *Pcyt2* has an intrinsic role in the regulation of liver lipid secretion, plasma lipolysis, and postprandial lipid metabolism.

Initially, we reported that older (32 week) *Pcyt2*^{-/-} mice have upregulated liver lipogenic genes, reduced FA oxidation,

and increased FFA uptake, and accumulate liver lipids and have characteristic lipoprotein profiles with elevated VLDL content and normal HDL and LDL content (16). Here, we have established that the liver VLDL-TAG secretion is not impaired in young animals, but becomes significantly elevated in older (32 week and 42 week) *Pcyt2*^{-/-} mice. Furthermore, we provide several lines of evidence that in addition to being hypertriglyceridemic, *Pcyt2*^{-/-} mice

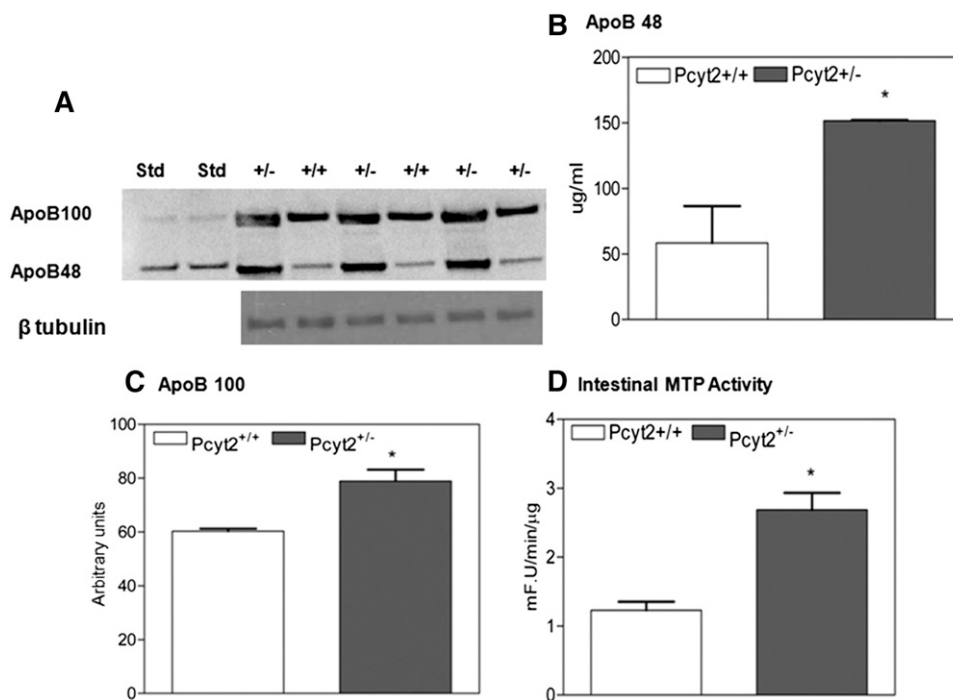


Fig. 6. *Pcyt2*^{-/-} mice have increased plasma apoB and intestinal MTP activity. A: Immunoblotting of *Pcyt2*^{-/-} and control plasma for apoB-48 and apoB-100 3 h after an intragastric load of 200 μ l of olive oil; β tubulin was used as a loading control. B,C: ApoB-48 and apoB-100 were dramatically elevated in *Pcyt2*^{-/-} plasma. D: MTP activity was upregulated in *Pcyt2*^{-/-} small intestine and was expressed as fluorescence U/min/ μ g protein (n = 5 and *P* < 0.05).

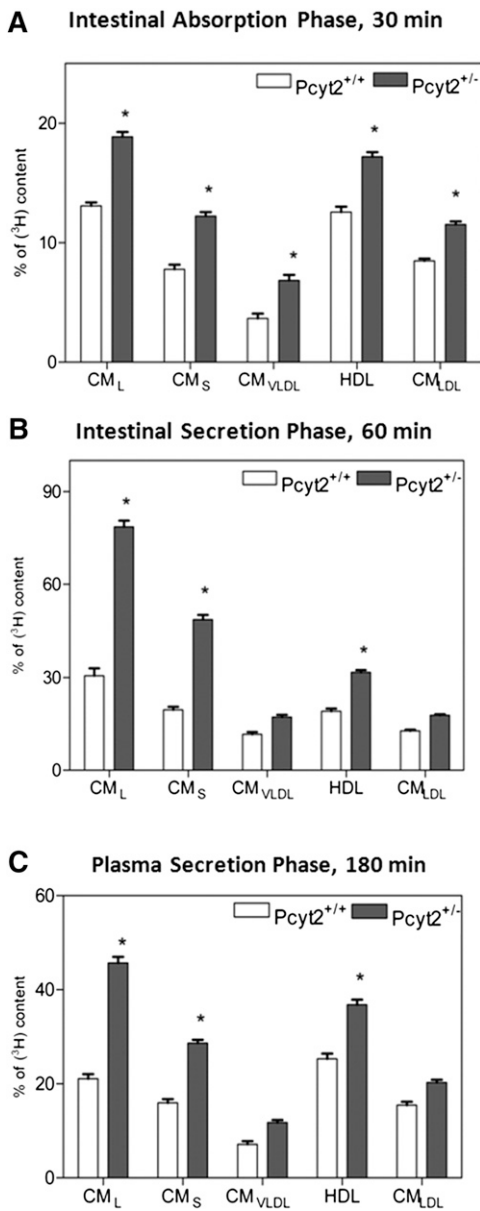


Fig. 7. Differences in lipidation of intestinally derived lipoproteins. A: Density profile of enterocyte lipoproteins immediately (30 min) after an intragastric load of [³H]TO. B: The enterocyte lipoproteins secreted 3 h after the [³H]TO load. C: Plasma lipoprotein profiles 1 h after the lipid load; values are shown for n = 5 and as percent of dpm/mg protein for enterocyte in A, B and percent dpm/ml for plasma in C. Statistical significance (*) between the two genotypes was determined by Student's *t*-test at *P* < 0.05.

additionally exhibit an increased capacity to process exogenous lipids in intestinal epithelial cells and have reduced capacity to clear postprandial lipids from circulation. Using an oral lipid tolerance test, we demonstrated that *Pcyt2*^{-/-} mice had significantly reduced turnover of circulating TAG compared with wild-type littermates. By separate examination of plasma TAG influx and degradation, we established that *Pcyt2*^{-/-} mice increase the processing of dietary lipids, as well as reduce plasma lipolysis, which together resulted in a longer TAG half-life in the plasma. We demonstrate that postprandial lipids appeared in *Pcyt2*^{-/-} circulation at rates faster than in the control littermates.

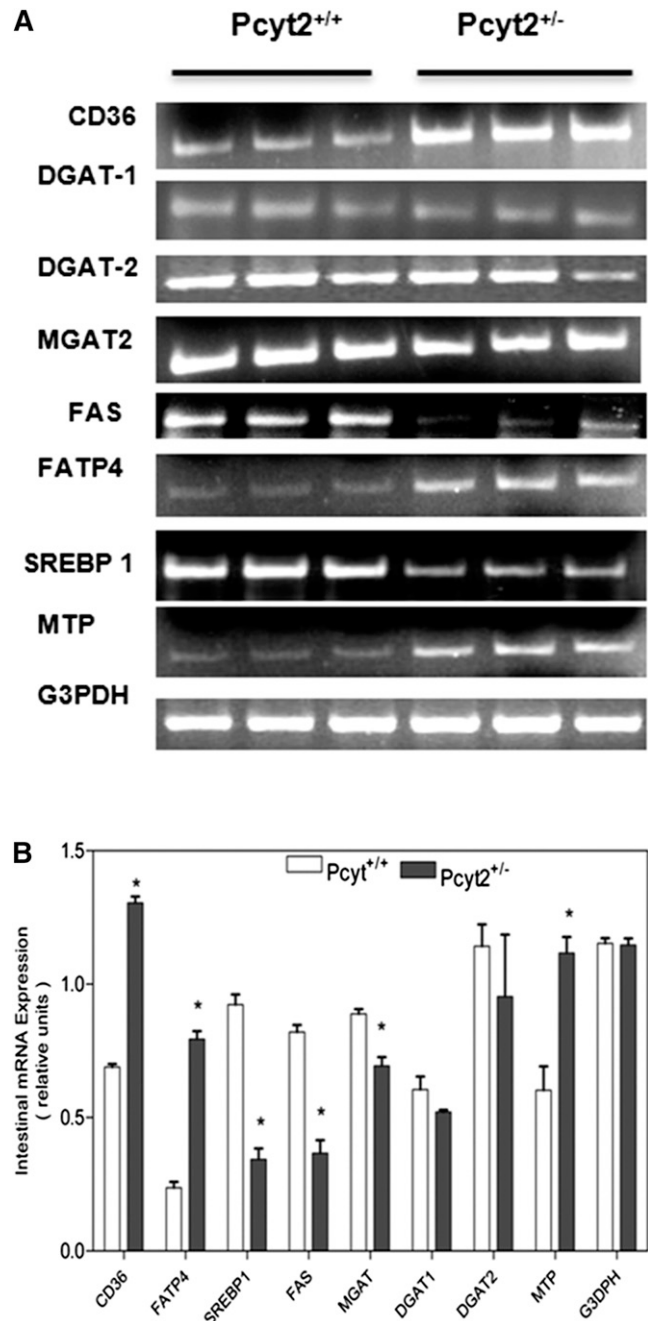


Fig. 8. Intestinal genes for lipid transport and chylomicron formation are overexpressed in *Pcyt2* deficiency. A: Representative RT-PCR expression data for the FA synthase (FAS), diacylglycerol transferase 1 and 2 (DGAT-1 and -2), monoacylglycerol acyltransferase (MGAT2), FATP4, FA transporter CD36, sterol-regulatory binding protein 1 (SREBP1), microsomal transfer protein (MTP), and glycerol-3-phosphate dehydrogenase (G3PDH) loading control in *Pcyt2*^{-/-} and *Pcyt2*^{+/+} small intestine. B: Average mRNA band densities from at least three separate RNA isolations in each group of animals. Statistical significance (*) between the two genotypes was determined by Student's *t*-test at *P* < 0.05.

Lipoprotein density fractionation established that *Pcyt2*^{-/-} enterocytes and plasma had substantially increased lipidation of chylomicron particles, and that increased chylomicron production in *Pcyt2* deficiency was accompanied by an abundant presence of apoB-48 in the plasma. Finally, the facilitated processing of dietary lipids in *Pcyt2*^{-/-} intestine

was supported by elevated expression and/or activity of intestinal genes responsible for FA transport and esterification (CD36 and FATP4 expression) and chylomicron assembly and secretion (increased MTP gene expression and activity). An additional possibility for the facilitation of intestinal lipid uptake may be that digested products (FFA, DAG, and MAG) also experience a lower barrier to absorption, linked to modified membrane fluidity and composition. *Pcyt2*^{+/-} mice have normal membrane PC/PE and cholesterol/phospholipid ratios; however, the elevated saturated and monounsaturated FAs and reduced content of PUFAs in the membrane PE (8) may be significant. Whether this uniquely modified PE content modifies membrane lipid absorption remains unknown.


In addition to pronounced lipogenesis and reduced FA oxidation, older *Pcyt2*^{+/-} mice also have increased uptake of circulating FFAs, the processes we initially found to be responsible for development of hepatic steatosis (16). The elevated expression of lipogenic genes SREBP1 and FAS in the *Pcyt2*^{+/-} liver cells could be normalized by fully restoring the *Pcyt2* expression and function (17). Interestingly, intestinal lipogenesis was reduced in *Pcyt2*^{+/-} mice, as was shown by lower expression of the key lipogenic genes SREBP1 and FAS, further indicating that excess FAs absorbed from diet (33), not synthesized de novo from glucose, constituted the bulk of the intracellular FA pool used for the chylomicron formation. Therefore, it is apparent that *Pcyt2* deficiency differently influenced FA and glucose metabolism in liver and intestine and that the metabolic disturbances in multiple organs contributed to the development of the *Pcyt2*^{+/-} mice hyperlipidemia.

The abnormalities in lipoprotein turnover were evident from reduced plasma lipid degradation and from reduced lipid uptake in multiple *Pcyt2*^{+/-} tissues. The extended half-life of circulating TAG was accompanied by a 50% reduction in liver and adipose tissue uptake in *Pcyt2*^{+/-} mice. These data agree with our previous report, suggesting unchanged liver TAG degradation by lipolysis (16), and also that receptor-mediated lipoprotein uptake could be impaired in the *Pcyt2*^{+/-} liver and adipocytes. The impaired catabolism of plasma TAG in *Pcyt2*^{+/-} mice was also a result of reduced postheparin LPL and HL activities. The molecular mechanisms for the reduced activities of LPL and HL in *Pcyt2*^{+/-} mice implicate factors other than the product inhibition by FFAs, because we previously established that *Pcyt2*-deficient animals had only mildly elevated FFA content in the plasma (16). We showed that downregulation of plasma LPL in *Pcyt2*^{+/-} mice was caused by reduced LPL mRNA in adipose tissue and heart, and we identified that the potent LPL inhibitor Angptl4 was abundant in *Pcyt2*^{+/-} plasma. These changes probably contribute to the reduced LPL activity and *Pcyt2*^{+/-} hyperlipidemia, but other factors, such as apoC-III and the LPL transport protein glycosyl phosphatidylinositol-anchored HDL binding protein 1 are likely to have additionally altered the LPL content and activity (38–40).

HL is released from the liver, and the HL activity in the plasma is predominantly regulated by the HDL content and composition. HL can also control the VLDL TAG pool in both humans and mice (41, 42). The HL activity was significantly

reduced in *Pcyt2*^{+/-} plasma, implicating additional complications in HDL secretion and/or plasma composition in *Pcyt2*^{+/-} mice. Plasma TAG FA composition is significantly modified in heterozygous mice, containing elevated content of C16 and C18 n-6 FAs (16), probably the products of the elevated *Pcyt2*^{+/-} mice intestinal absorption, but also increased liver VLDL secretion and lipogenesis (16, 17). Future studies on the regulation of the specific contributions of liver and intestinal lipoproteins and lipoprotein receptors in *Pcyt2* deficiency will help in better understanding the mechanisms driving the impaired plasma lipid clearance and how lipases and regulatory proteins contribute to the accumulation of plasma TAG in *Pcyt2* deficiency.

The disruption of *Pcyt2* is responsible not only for altering TAG synthesis, but also for affecting other aspects of lipid homeostasis, such as FA oxidation and reduced PE availability as a source of FA (16, 17). *Pcyt2*^{+/-} mice also develop insulin resistance, even on a chow diet (16), which, together with the elevated postprandial lipids (also on a chow diet), imply that in mice chronically exposed to a high-fat diet regimen, reduced *Pcyt2* activity might also contribute a high-fat diet-induced hypertriglyceridemia and development of type-2 diabetes, as seen in humans. Based on our initial work discussed earlier and information from numerous diet-induced obesity models, we anticipate that the phenotype described here for the older *Pcyt2*^{+/-} mice would appear earlier in the life if young mice were fed a high-fat diet. Postprandial lipemia is a well-known risk factor for development of type-2 diabetes (43), and available data suggest that the expression of human *Pcyt2* is reduced in adipose tissue in women with polycystic ovary syndrome (44), in myotubes from patients with type-2 diabetes (45), and in MODY type-2 diabetes (46).

In conclusion, we establish that hypertriglyceridemia observed in the *Pcyt2*-heterozygous mouse can be attributed to elevated lipid secretion and over-production of TAG-rich particles. This, in combination with impaired lipolytic conversion of TAG-rich remnants, results in subsequent reduced delivery of TAG-derived lipids to peripheral tissues. The heterozygous disruption of *Pcyt2* results in aberrant lipid absorption and the age-related development of obesity and metabolic syndrome, which opens an interesting new area to be considered when studying lipid-related disorders, impairments in membrane phospholipid gene function, and phospholipid homeostasis. 

REFERENCES

1. Guo, Y., T. C. Walther, M. Rao, N. Stuurman, G. Goshima, K. Terayama, J. S. Wong, R. D. Vale, P. Walter, and R. V. Farese. 2008. Functional genomic screen reveals genes involved in lipid-droplet formation and utilization. *Nature*. **453**: 657–661.
2. Igal, R. A., J. M. Caviglia, I. N. De Gomez Dumm, and R. A. Coleman. 2001. Diacylglycerol generated in CHO cell plasma membrane by phospholipase C is used for triacylglycerol synthesis. *J. Lipid Res.* **42**: 88–95.
3. Caviglia, J. M., I. N. De Gomez Dumm, R. A. Coleman, and R. A. Igal. 2004. Phosphatidylcholine deficiency upregulates enzymes of triacylglycerol metabolism in CHO cells. *J. Lipid Res.* **45**: 1500–1509.
4. Vance, D. E. 2008. Role of phosphatidylcholine biosynthesis in the regulation of lipoprotein homeostasis. *Curr. Opin. Lipidol.* **19**: 229–234.
5. Vance, D. E., and J. E. Vance. 2009. Physiological consequences of disruption of mammalian phospholipid biosynthetic genes. *J. Lipid Res.* **50** (Suppl.): S132–137.

6. Li, Z., L. B. Agellon, T. M. Allen, M. Umeda, L. Jewell, A. Mason, and D. E. Vance. 2006. The ratio of phosphatidylcholine to phosphatidylethanolamine influences membrane integrity and steatohepatitis. *Cell Metab.* **3**: 321–331.
7. Fu, S., L. Yang, P. Li, O. Hofmann, L. Dicker, W. Hide, X. Lin, S. M. Watkins, A. R. Ivanov, and G. S. Hotamisligil. 2011. Aberrant lipid metabolism disrupts calcium homeostasis causing liver endoplasmic reticulum stress in obesity. *Nature.* **473**: 528–531.
8. Fullerton, M. D., F. Hakimuddin, and M. Bakovic. 2007. Developmental and metabolic effects of disruption of the mouse CTP:phosphoethanolamine cytidyltransferase gene (Pcyt2). *Mol. Cell Biol.* **27**: 3327–3336.
9. Bakovic, M., M. D. Fullerton, and V. Michel. 2007. Metabolic and molecular aspects of ethanolamine phospholipid biosynthesis: the role of CTP:phosphoethanolamine cytidyltransferase (Pcyt2). *Biochem. Cell Biol.* **85**: 283–300.
10. Hermansson, M., K. Hokynar, and P. Somerharju. 2011. Mechanisms of glycerophospholipid homeostasis in mammalian cells. *Prog. Lipid Res.* **50**: 240–257.
11. Poloumienko, A., A. Cote, A. Q. Tie, L. Zhu, and M. Bakovic. 2004. Genomic organization and differential splicing of the mouse and human Pcyt2 genes. *Gene.* **325**: 145–155.
12. Tie, A., and M. Bakovic. 2007. Alternative splicing of CTP:phosphoethanolamine cytidyltransferase produces two isoforms that differ in catalytic properties. *J. Lipid Res.* **48**: 2172–2181.
13. Johnson, C. M., Z. Yuan, and M. Bakovic. 2005. Characterization of transcription factors and cis-acting elements that regulate human CTP:phosphoethanolamine cytidyltransferase (Pcyt2). *Biochim. Biophys. Acta.* **1735**: 230–235.
14. Zhu, L., V. Michel, and M. Bakovic. 2009. Regulation of the mouse CTP:phosphoethanolamine cytidyltransferase gene Pcyt2 during myogenesis. *Gene.* **447**: 51–59.
15. Zhu, L., and M. Bakovic. 2008. Liver X receptor agonists inhibit the phospholipid regulatory gene CTP:phosphoethanolamine cytidyltransferase-Pcyt2. *Biochem. Res. Int.* **2008**: 801849.
16. Fullerton, M. D., F. Hakimuddin, A. Bonen, and M. Bakovic. 2009. The development of a metabolic disease phenotype in CTP:phosphoethanolamine cytidyltransferase deficient mice. *J. Biol. Chem.* **284**: 25704–25713.
17. Fullerton, M., and M. Bakovic. 2010. Complementation of the metabolic defect in CTP:phosphoethanolamine cytidyltransferase (Pcyt2) deficient primary hepatocytes. *Metabolism.* **59**: 1691–1700.
18. Leonardi, R., M. W. Frank, P. D. Jackson, C. O. Rock, and S. Jackowski. 2009. Elimination of the CDP-ethanolamine pathway disrupts hepatic lipid homeostasis. *J. Biol. Chem.* **284**: 27077–27089.
19. Millar, J. S., D. A. Cromley, M. G. McCoy, D. J. Rader, and J. T. Billheimer. 2005. Determining hepatic triglyceride production in mice: comparison of poloxamer 407 with Triton WR-1339. *J. Lipid Res.* **46**: 2023–2028.
20. Johnston, T. P. 2010. Poloxamer 407 as a general lipase inhibitor: its implication in lipid metabolism and atheroma formation in C57BL/6 mice. *J. Pharm. Pharmacol.* **62**: 1807–1812.
21. Bligh, E. G., and W. J. Dyer. 1959. A rapid method of total lipid extraction and purification. *Can. J. Med. Sci.* **37**: 911–917.
22. Goudriaan, J. R., S. M. S. E. Santo, P. J. Voshol, and P. C. Rensen. 2004. The VLDL receptor plays a major role in chylomicron metabolism by enhancing LPL-mediated triglyceride hydrolysis. *J. Lipid Res.* **45**: 1475–1481.
23. Moen, C. J., A. P. Tholens, P. J. Voshol, and P. C. Rensen. 2007. The Hyplip2 locus causes hypertriglyceridemia by decreased clearance of triglycerides. *J. Lipid Res.* **48**: 2182–2192.
24. Vine, D. F., R. Takechi, J. C. Russell, and S. D. Proctor. 2007. Impaired postprandial apolipoprotein-B48 metabolism in the obese, insulin-resistant JCR:LA-cp rat: increased atherogenicity for the metabolic syndrome. *Atherosclerosis.* **190**: 282–290.
25. Swift, L. L., A. Jovanovska, B. Kakkad, and D. E. Ong. 2005. Microsomal triglyceride transfer protein expression in mouse intestine. *Histochem. Cell Biol.* **123**: 475–482.
26. Cheng, D., J. Iqbal, J. Devenny, C-H. Chu, L. Chen, J. Dong, R. Seethala, W. J. Keim, A. V. Azzara, R. M. L. Lawrence, et al. 2008. Acylation of acylglycerols by acyl coenzyme A:diacylglycerol acyltransferase 1 (DGAT1). Functional importance of DGAT1 in the intestinal fat absorption. *J. Biol. Chem.* **283**: 29802–29811.
27. Luchoomun, J., and M. M. Hussain. 1999. Assembly and secretion of chylomicrons by differentiated Caco-2 cells. Nascent triglycerides and preformed phospholipids are preferentially used for lipoprotein assembly. *J. Biol. Chem.* **274**: 19565–19572.
28. Nayak, N., E. H. Harrison, and M. M. Hussain. 2001. Retinyl ester secretion by intestinal cells: a specific and regulated process dependent on assembly and secretion of chylomicrons. *J. Lipid Res.* **42**: 272–280.
29. Anwar, K., H. J. Kayden, and M. M. Hussain. 2006. Transport of vitamin E by differentiated Caco-2 cells. *J. Lipid Res.* **47**: 1261–1273.
30. Iqbal, J., and M. M. Hussain. 2005. Evidence for multiple complementary pathways for efficient cholesterol absorption in mice. *J. Lipid Res.* **46**: 1491–1501.
31. Lu, B., A. Moser, J. K. Shigenaga, C. Grunfeld, and K. R. Feingold. 2010. The acute phase response stimulates the expression of angiotensin like protein 4. *Biochem. Biophys. Res. Commun.* **391**: 1737–1741.
32. Yen, C. L., S. J. Stone, S. Koliwad, C. Harris, and R. V. Farese, Jr. 2008. DGAT enzymes and triacylglycerol biosynthesis. *J. Lipid Res.* **49**: 2283–2301.
33. Hsieh, J., C. Longuet, A. Maida, J. Bahrami, E. Xu, C. L. Baker, and K. Adeli. 2009. Glucagon-like peptide-2 increases intestinal lipid absorption and chylomicron production via CD36. *Gastroenterology.* **137**: 997–1005.
34. De Guzman, J. M., G. Ku, R. Fahey, Y. H. Youm, I. Kass, D. K. Ingram, V. D. Dixit, and I. Kheterpal. Chronic caloric restriction partially protects against age-related alteration in serum metabolome. *Age (Dordr.)*. Epub ahead of print. June 4, 2012. DOI 10.1007/s11357-012-9430-x.
35. Sample, J., J. G. Cleland, and A. M. Seymour. 2006. Metabolic remodeling in the aging heart. *J. Mol. Cell. Cardiol.* **40**: 56–63.
36. Ming, X. F., J. P. Montani, and Z. Yang. 2012. Perspectives of Targeting mTORC1–S6K1 in cardiovascular aging. *Front Physiol.* **3**: 5–11.
37. Kapahi, P., D. Chen, A. N. Rogers, S. D. Katewa, P. W. Li, E. L. Thomas, and L. Kockel. 2010. With TOR, less is more: a key role for the conserved nutrient-sensing TOR pathway in aging. *Cell Metab.* **11**: 453–465.
38. Lichtenstein, L., and S. Kersten. 2010. Modulation of plasma TG lipolysis by angiotensin-like proteins and GPIHBP1. *Biochim. Biophys. Acta.* **1801**: 415–420.
39. Dallinga-Thie, G. M., R. Franssen, H. L. Mooij, M. E. Visser, H. C. Hassing, F. Peelman, J. J. Kastelein, M. Péterfy, and M. Nieuwdorp. 2010. The metabolism of triglyceride-rich lipoproteins revisited: new players, new insight. *Atherosclerosis.* **211**: 1–8.
40. Davies, B. S., A. P. Beigneux, L. G. Fong, and S. G. Young. 2012. New wrinkles in lipoprotein lipase biology. *Curr. Opin. Lipidol.* **23**: 35–42.
41. Chatterjee, C., and D. L. Sparks. 2011. Hepatic lipase, high density lipoproteins, and hypertriglyceridemia. *Am. J. Pathol.* **178**: 1429–1433.
42. Pratt, S. M., S. Chiu, G. M. Espinal, N. M. Shibata, H. Wong, and C. H. Warden. 2010. Mouse hepatic lipase alleles with variable effects on lipoprotein composition and size. *J. Lipid Res.* **51**: 1035–1048.
43. Hsieh, J., A. A. Hayashi, J. Webb, and K. Adeli. 2008. Postprandial dyslipidemia in insulin resistance: mechanisms and role of intestinal insulin sensitivity. *Atheroscler. Suppl.* **9**: 7–13.
44. Cortón, M., J. I. Botella-Carretero, A. Benguría, A. Villuendas Zaballos, J. L. San Millán, H. F. Escobar-Morreale, and B. Peral. 2007. Differential gene expression profile in omental adipose tissue in women with polycystic ovary syndrome. *J. Clin. Endocrinol. Metab.* **92**: 328–337.
45. Frederiksen, C. M., K. Højlund, L. Hansen, E. J. Oakeley, B. Hemmings, B. M. Abdallah, K. Brusgaard, H. Beck-Nielsen, and M. Gaster. 2008. Transcriptional profiling of myotubes from patients with type-2 diabetes: no evidence for a primary defect in oxidative phosphorylation genes. *Diabetologia.* **51**: 2068–2077.
46. Lee, Y. H., S. Nair, E. Rousseau, D. B. Allison, G. P. Page, P. A. Tataranni, C. Bogardus, and P. A. Permana. 2005. Microarray profiling of isolated abdominal subcutaneous adipocytes from obese vs non-obese Pima Indians: increased expression of inflammation-related genes. *Diabetologia.* **48**: 1776–1783.